Pergamon

Cement and Concrete Research 30 (2000) 1929–1939

CEMENT AND CONCRETE RESEARCH

Modeling the deterioration of hydrated cement systems exposed to frost action
Part 1: Description of the mathematical model

B. Zuber[a,b], J. Marchand[a,*]

[a]*CRIB-Département de génie civil, Université Laval, Sainte-Foy, Québec, Canada, G1K 7P4*
[b]*LMT-Ecole normale supérieure de Cachan, 61, avenue du Président Wilson, Cachan Cedex, France*

Received 17 February 2000; accepted 31 July 2000

Abstract

The main features of a numerical model predicting the behavior of hydrated cement systems subjected to freezing temperatures are presented. The model is derived from thermodynamic and kinetic considerations. All equations are written at the microscopic scale and then averaged over an elementary representative volume of the material (mesoscopic scale). The system of equations is built in such a way as to predict temperature-induced phase transitions and the resulting transfer of mass within the material pore structure. The model also yields the local pressures generated in the liquid and solid phases by mass transfer and crystal growth. The system of non-linear equations is solved numerically. A complete description of the input data required to run the model is given. The last section includes a discussion of the various assumptions forming the basis of the model. Part II of this series will be devoted to a systematic comparison of the numerical results to experimental data.

Keywords: Modeling; Freezing and thawing; Transport properties; Kinetics; Pore size distribution; Cement; Concrete; Frost durability; Ice formation; Service life

1. Introduction

Concrete, like other highly divided porous media, has the ability to absorb and retain moisture. This characteristic has an important consequence since unprotected concrete structures in contact with water are usually susceptible to frost damage. It has been clearly established that saturated concrete exposed to repeated freezing and thawing cycles can be affected by two types of deterioration: internal microcracking and de-icer salt scaling (also known as surface scaling) [1]. It has also been shown that, in practice, each phenomenon can occur independently of the other.

Given the importance of these problems, significant effort has been made on understanding the basic mechanisms that control the resistance of concrete to both types of degradation. Generally, internal microcracking and de-icer salt scaling are considered to be two distinct manifestations of the same degradation mechanism [2,3]. In both cases, damage is attributed to local stresses resulting from the growth of ice crystals and internal pressures induced by the transfer of liquid water [2,4,5].

Historically, moisture movement within the material pore structure has been attributed to the expulsion of unfrozen water from the freezing sites. The phenomenon was associated with the 9% expansion of water upon freezing (the so-called hydraulic pressure theory) [6]. Convincing evidence of the subsequent migration of unfrozen water to the freezing sites was later reported by numerous researchers [7–9]. The driving force for this ice accretion phenomenon was linked to the existence of a free energy gradient between ice and unfrozen water. A similar mechanism is often proposed to explain heaving problems in frozen soils [10,11].

Recent surveys indicate that none of the proposed theories can account for the full body of experimental results reported in the literature [1,12]. In practice, this lack of basic understanding has significantly affected the work of civil

* Corresponding author. Tel.: +1-418-656-2079; fax: +1-418-656-3355.
E-mail address: jmarchan@gci.ulaval.ca (J. Marchand).

0008-8846/00/$ – see front matter
PII: S0008-8846(00)00405-1

engineers and concrete technologists. For instance, there still exists no reliable solution to fully protect normal concrete structures against de-icer salt scaling [1,12,13].

Although air entrainment is highly beneficial to the de-icer salt scaling resistance of concrete, both field experience and laboratory tests show that deterioration often still occurs in properly air-entrained concrete mixtures [14]. Laboratory investigations also indicate that silane- and siloxane-based sealers, generally used to prevent the ingress of chloride ions and reduce the risk of reinforcement corrosion, cannot protect concrete structures against salt scaling [15].

It has also been clearly established that certain types of concrete mixtures can also be susceptible to internal microcracking. This is, for instance, the case for some dry concrete (e.g., roller-compacted concrete, concrete paving blocks, etc.) and high-performance concrete mixtures that cannot always benefit from the protection of a properly entrained air-void network [16–19]. Recent experience indicates that air entrainment in these low water/binder ratio (and high viscosity) mixtures can be difficult to achieve in practice [17,20].

A detailed description of a model aimed at predicting the behavior of hydrated cement systems exposed to freezing temperatures is given in the following sections. The general framework of the model was inspired by the earlier work of Bažant et al. [21] and Scherer [3–5]. The model is derived from thermodynamic and kinetic considerations. The multi-scale character of the problem is taken into account. Some equations are written at the microscopic scale and then homogenized over an elementary representative volume of the material (mesoscopic scale). The system of equations is constructed to quantitatively predict the mass transfer phenomena within the material pore structure. The model also allows the calculation of local pressures generated in the liquid and solid phases by mass transfer and crystal growth. Part II will be devoted to a systematic comparison of the numerical results to published experimental data.

2. Research significance

The existing lack of understanding of the fundamental mechanisms involved in the de-icer salt scaling and internal microcracking of concrete clearly emphasizes the complex nature of these phenomena. The imperfect knowledge of these problems has impeded the development of reliable and practical solutions. It has also limited the ability to design relevant accelerated test methods.

The development of models based on thermodynamic considerations and a precise description of the physical properties of hydrated cement systems will hopefully contribute to improve the knowledge of the mechanisms of frost damage. The model presented in the following sections has been designed to investigate the degradation phenomena at the scale of the material. It should provide information on the critical parameters that control the resistance of cement-based materials to internal microcracking. The detrimental influence of dissolved salts is not addressed here and will be the subject of a separate publication. Future work will also be devoted to the description of the macroscopic behavior of concrete exposed to freezing and thawing cycles [22]. This last part of the study will be specifically dedicated to the prediction of the evolution of various phenomena (e.g., saturation, temperature field and cumulative mechanical damage) and the treatment of boundary conditions.

3. Theoretical background

3.1. Mass balance equations

The phenomena of fluid transfer in porous solids have been extensively investigated over the past decades [23–27]. In a poro-elastic approach [21,28,29], the mass balance, with phase change phenomena, of fluids in the porous medium may be described by the following equation:

$$\frac{\partial}{\partial t}(nS_{\mathrm{l}}\rho_{\mathrm{l}}) + \mathrm{div}(nS_{\mathrm{l}}\rho_{\mathrm{l}}\boldsymbol{u}_{\mathrm{l}}) = \frac{-1}{V}\frac{\mathrm{d}m_{\mathrm{l}\rightarrow\mathrm{i}}}{\mathrm{d}t} \tag{1}$$

ρ_{l} is the liquid water density and $\boldsymbol{u}_{\mathrm{l}}$ is the absolute velocity vector of the fluid particles. In the previous equation, n represents the total porosity of the porous material and S^{i} stands for the fraction of the pore volume filled with phase j. In the present case, it is assumed that only two fluids are present in the porosity: liquid water (identified by the subscript l) and ice (identified by the subscript i). Accordingly, the following relation [Eq. (2)] must always be verified:

$$S_{\mathrm{l}} + S_{\mathrm{i}} = 1 \tag{2}$$

The source/sink term $((-1)/(V))((\mathrm{d}m_{\mathrm{l}\rightarrow\mathrm{i}})/(\mathrm{d}t))$ in Eq. (1) accounts for any consumption or production of liquid water within the material. For instance, it can be used to take into consideration the influence of various phenomena such as drying and hydration. In the following sections, this term will be used to describe the effect of ice formation on the mass transfer of liquid water. Its expression will be discussed in Section 3.2.1. A similar description of fluid transfer problems in porous media has been used to study the behavior of concrete exposed to high temperature [30] and to investigate the mechanisms of strain localization in geomaterials [31].

The velocity of the fluid particles, $\boldsymbol{u}_{\mathrm{l}}$, may be expressed in terms of the solid skeleton velocity, $\boldsymbol{u}$, and the flux of fluid, $\boldsymbol{j}_{\mathrm{l}}$, in the porous network (the latter representing the relative velocity between the liquid water and the solid skeleton):

$$\boldsymbol{u}_{\mathrm{l}} = \boldsymbol{u} + \frac{\boldsymbol{j}_{\mathrm{l}}}{nS_{\mathrm{l}}} \tag{3}$$

The fluid flux [Eq. (3)] can be related to the pressure gradient using Darcy's law (describing a fluid flow essentially laminar) [28,29];

$$\boldsymbol{j}_{\mathrm{l}} = -\frac{D}{\eta_{\mathrm{l}}}\mathrm{grad}p_{\mathrm{l}} \tag{4}$$

with D being the permeability of the porous medium and η_{l} the dynamic viscosity of liquid water.

In an eulerian description, one can write the particulate derivative of a quantity g with respect to the solid skeleton particles as [Eq. (5)]:

$$\frac{\mathrm{d}g}{\mathrm{d}t} = \frac{\partial g}{\partial t} + \boldsymbol{u}\mathrm{grad}g \tag{5}$$

then, Eq. (1) becomes:

$$\frac{n}{\rho_{\mathrm{l}}}\frac{\mathrm{d}\rho_{\mathrm{l}}}{\mathrm{d}t} + \frac{n}{S_{\mathrm{l}}}\frac{\mathrm{d}S_{\mathrm{l}}}{\mathrm{d}t} + \frac{\mathrm{d}n}{\mathrm{d}t} + \frac{1}{S_{\mathrm{l}}}\mathrm{div}\boldsymbol{j}_{\mathrm{l}} + \frac{\boldsymbol{j}_{\mathrm{l}}}{S_{\mathrm{l}}\rho_{\mathrm{l}}}\mathrm{grad}\rho_{\mathrm{l}} = \frac{-1}{S_{\mathrm{l}}\rho_{\mathrm{l}}}\frac{1}{V}\frac{\mathrm{d}m_{\mathrm{l}\to\mathrm{i}}}{\mathrm{d}t} \tag{6}$$

The mass balance equations of ice and of the solid phase that forms the porous skeleton can be more easily developed. If it is assumed that ice does not flow through the porous network, then ice and solid particles have the same absolute velocity at each time, $\boldsymbol{u}$. For the solid phase, one finds that:

$$\frac{(1-n)}{\rho_{\mathrm{s}}}\frac{\mathrm{d}\rho_{\mathrm{s}}}{\mathrm{d}t} - \frac{\mathrm{d}n}{\mathrm{d}t} + (1-n)\mathrm{div}\boldsymbol{u} = 0 \tag{7}$$

For ice, the source/sink term corresponding to the phase change is the same than that appearing in the mass balance equation of liquid water [Eq. (6)]. However, since liquid water is transformed in ice, and reversely, the sign of the term has to be changed. Hence, one finds:

$$\frac{n}{\rho_{\mathrm{i}}}\frac{\mathrm{d}\rho_{\mathrm{i}}}{\mathrm{d}t} + \frac{n}{S_{\mathrm{i}}}\frac{\mathrm{d}S_{\mathrm{i}}}{\mathrm{d}t} + \frac{\mathrm{d}n}{\mathrm{d}t} = \frac{+1}{S_{\mathrm{i}}\rho_{\mathrm{i}}}\frac{1}{V}\frac{\mathrm{d}m_{\mathrm{l}\to\mathrm{i}}}{\mathrm{d}t} \tag{8}$$

3.2. Phase change phenomena

3.2.1. Description of the ice formation process

Many investigations have shown that spontaneous nucleation is unlikely to govern the liquid/solid phase transition in hydrated cement systems [4,32,33]. The ice formation process is rather characterized by the propagation of a curved liquid/solid interface, initiated from external surfaces or large voids, which gradually penetrates the solid pore structure as the ambient temperature decreases below the triple point of water.

The propagation of this interface is controlled by the material pore size distribution (see Fig. 1) [3,4]. Using thermodynamic arguments, it can be shown that the formation of ice is limited by the curvature $R_{\mathrm{eq}}(T)$ of the liquid/solid interface [3,4,19]. This phenomenon is described by the following equation [32]:

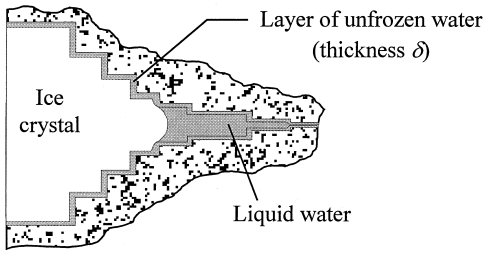

Fig. 1. Propagation of an ice front in a porous medium.

$$R_{\mathrm{eq}}(T) = \frac{2\gamma_{\mathrm{li}}(T)}{\int_{T_0}^{T}\frac{\Delta s_{\mathrm{li}}(T)}{v_{\mathrm{l}}}} \tag{9}$$

where γ_{li} is the surface tension of the liquid/ice interface, Δs_{li} is the entropy of ice formation, and v_{l} is the molar volume of the liquid phase. As indicated in the equation, γ_{li} and Δs_{li} are both temperature-dependent variables. The variation of Δs_{li} is discussed in the last section of this paper. More information on the evaluation of Δs_{li} can be found in Ref. [19].

Hence, at a given temperature T, there exists a critical pore radius $R_{\mathrm{p_{eq}}}$ below which ice cannot be formed. The value of this critical pore radius is given by the following equation:

$$R_{\mathrm{p_{eq}}}(T) = R_{\mathrm{eq}}(T) + \delta(T) \tag{10}$$

where $R_{\mathrm{eq}}(T)$ is the radius of curvature of the liquid/ice interface and $\delta(T)$ is the thickness of the liquid-like layer of adsorbed water that remains unfrozen on the pore walls during the ice formation process (see Fig. 1). As indicated by Eq. (10), the thickness of this unfrozen layer tends to vary with temperature. According to Fagerlund [34], its value, expressed in nanometers, can be estimated by the following relation:

$$\delta(\theta) = 1.97\sqrt[3]{\frac{1}{|\theta|}} \tag{11}$$

where θ is the temperature expressed in degrees Celsius. The variation of δ with temperature is illustrated in Fig. 2. As can be seen, at -25°C, the value of δ is 0.7 nm. This result is in good agreement with the experimental data of Bager and Sellevold [35] and those of Radjy [36]. In both studies, the value of δ was estimated to be approximately 1 nm (i.e., approximately 3 BET-equivalent monolayers).

Fagerlund [18] has reported that the unfrozen layer has a relatively limited impact on the value of $R_{\mathrm{eq}}(T)$ over the temperature range 0°C to -25°C. However, the presence of this layer can have a significant influence at low temperatures, i.e., when ice tends to penetrate the smaller pores (see Fig. 2). Eq. (11) predicts an infinite value at

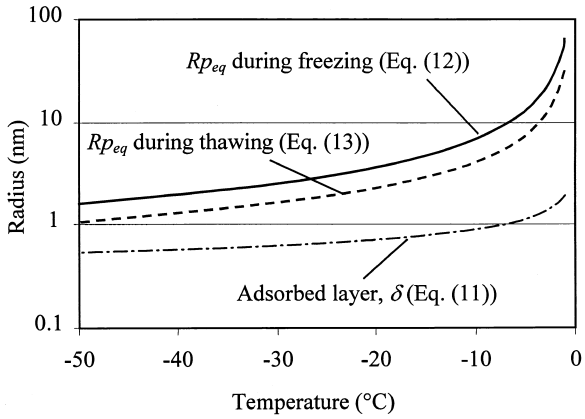

Fig. 2. Variation of the parameters δ and $R_{p_{eq}}$ as a function of temperature.

0°C. However, ice appearing first in largest pores and a few degrees below 0°C, one can consider this relation as a good approximation during the freezing process.

It should be emphasized that, given the intricate nature of the pore structure of hydrated cement systems, the value of $R_{p_{eq}}(T)$ determined for the freezing process should differ from that obtained for the thawing phase. As illustrated in Fig. 3, the value of $R_{p_{eq}}(T)$ upon freezing is determined by the dimension of the pore entry. During the thawing process, its value corresponds by the characteristic (maximum) radius of the pore. In this respect, the ice formation process is analogous to the injection of mercury during a porosimetry experiment [33,37–39]. Matala [32] proposed the following equations for the calculation of $R_{p_{eq}}(T)$ over the temperature range 0°C to −60°C:

$$\text{Freezing } (\dot{T}<0): \quad R_{p_{eq}} = 0.584 + 0.0052\ \theta - \frac{63.46}{\theta}\ \text{[nm]} \tag{12}$$

$$\text{Thawing } (\dot{T}>0): \quad R_{p_{eq}} = 0.757 + 0.0074\ \theta - \frac{33.45}{\theta}\ \text{[nm]} \tag{13}$$

The variation of $R_{p_{eq}}$ with temperature is illustrated in Fig. 2 for both the freezing and the thawing processes.

It should also be emphasized that Eqs. (12) and (13) were derived from thermodynamic (equilibrium) conditions. These equations do not account for supercooling effects (or any other non-equilibrium phenomena) that may occur during the freezing process.

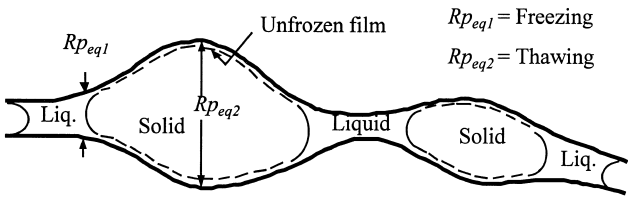

Fig. 3. Influence of the pore geometry on the mechanisms of freezing and thawing.

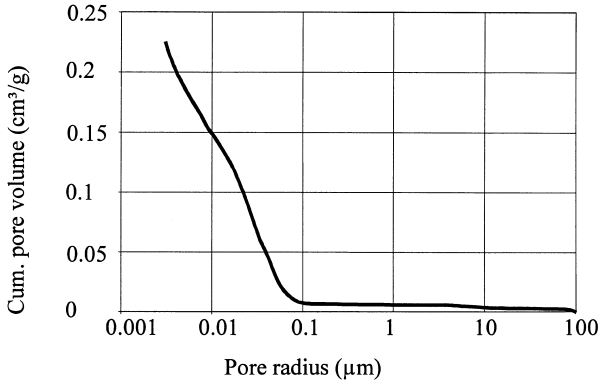

Fig. 4. Typical mercury intrusion pore size distribution ($\varphi(r)$) for a 0.7 water/cement ratio cement paste.

For a given pore size distribution (see, for instance, Fig. 4), the cumulative volume $\varphi(r)$ of pores with a radius greater than r is given by:

$$\varphi(r) = \int_r^{\infty} \frac{\mathrm{d}\varphi}{\mathrm{d}r}\mathrm{d}r \tag{14}$$

In the Eq. (14), the value of $\varphi(r)$ is expressed in cubic meters of pore per cubic meter of paste.

As previously discussed by Zuber et al. [19], the formation of ice in a porous solid can be theoretically predicted on the basis of its pore size distribution (as defined by Eq. (14)). Assuming that the freezing rate is sufficiently low (i.e., the rate of the ice formation is solely controlled by the rate of freezing),[1] the volume of ice formed during a given time increment can be calculated using the following equation:

$$\frac{1}{V}\frac{\mathrm{d}V_{\mathrm{l}\to\mathrm{i}}}{\mathrm{d}t} = \int_{R_{p_{eq}}(t)}^{R_{p_{eq}}(t+\mathrm{d}t)} \frac{\mathrm{d}\varphi}{\mathrm{d}r}(1 - v_{ads}(r))\mathrm{d}r \tag{15}$$

The volume of adsorbed water at temperature $T(t)$ may simply be evaluated by:

$$v_{ads}(T) = v_{ads}(R_{p_{eq}}(t)) = \int_{R_{p_{eq}}(t)}^{\infty} \frac{\mathrm{d}\varphi}{\mathrm{d}r} g(r,\delta)\mathrm{d}r \tag{16}$$

with the function g depending on the shape of the pore (Eq. (17)):

$$g(r,\delta) = 1 - \left(1 - \frac{\delta}{r}\right)^2 \text{ for cylindrical pores}$$
$$= 1 - \left(1 - \frac{\delta}{r}\right)^3 \text{ for spherical pores} \tag{17}$$

[1] It should be emphasized that this corresponds to the situation found in most practical cases where concrete structures are subjected to relatively slow freezing rates.

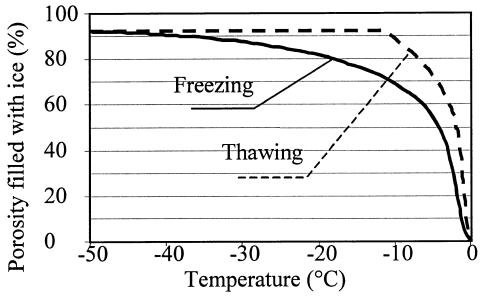

Fig. 5. Cumulative volume of ice predicted by Eqs. (12) and (13) for the 0.7 water/cement ratio paste (see Fig. 3).

It is apparent that the pore shape has some influence on the volume of unfrozen water. However, this influence is marginal since for $r = R_{p_{eq}}$, one can find that the value of the function g calculated for a spherical pore is lower than 1.5 times the value of g obtained for a cylindrical pore for temperatures within the range of validity of Eq. (12).

Then, with Eq. (16), Eq. (15) may be rewritten:

$$\frac{1}{V}\frac{dV_{l\to i}}{dt} = \int_{R_{p_{eq}}(t)}^{R_{p_{eq}}(t+dt)} \frac{d\varphi}{dr}(1 - g(r,\delta))dr = \Phi(t) \tag{18}$$

The prediction of the ice formation process requires a prior knowledge of the size distribution of the connected pore volume of the material. It has been shown that the pore size distribution of most hydrated cement systems (at least those with a water/cement ratio ≥ 0.40) can be reasonably well determined on the basis of mercury intrusion porosimetry (MIP) [37,38]. An ice formation curve (based on a MIP pore size distribution) for a 0.7 water/cement ratio paste is given in Fig. 5. Detailed discussions of the use of MIP test results for the prediction of the amount of ice formed in cement systems can be found in Refs. [19,32].

Finally, one can note that the value of the term $((1)/(V))((dm_{l\to i})/(dt))$ corresponds to the mass of liquid water that has frozen and filled the volume $dV_{l\to i}$ during the increment of time dt. Accordingly, one finds:

$$\frac{1}{V}\frac{dm_{l\to i}}{dt} = \rho_i \frac{1}{V}\frac{dV_{l\to i}}{dt} = \rho_i \Phi(t) \tag{19}$$

3.2.2. Pressures exerted on the pore walls

In the present case, the ice formed in the pore structure can be considered as a continuous phase. Furthermore, it can be assumed that the pressure $p_i(t)$ in the crystal is essentially controlled by the liquid/ice interface (the two phases are in mechanical equilibrium and offer a large surface of contact). Accordingly, one can write:

$$p_i(t) = p_l(t) + \kappa(t) \tag{20}$$

The second term on the right-hand side of the equation, κ, accounts for the effects of the spherical interface between liquid water and ice. Its value is given by Laplace equation:

$$\kappa(t) = \frac{2\gamma_{li}(t)}{R_{eq}(t)} \tag{21}$$

The penetration of an ice crystal into a pore of radius r modifies the value of the stress applied on the solid. As demonstrated by Scherer [4], this increase in stress is equal to [Eq. (22)]:

$$\chi(r,t) = \frac{\gamma_{li}(t)}{r - \delta(t)} \tag{22}$$

According to Scherer [4], the pressure $\pi_i(r,t)$ exerted by the ice crystal on the wall of a pore of radius r can be calculated by the following equation:

$$\pi_i(r,t) = p_l(t) + \chi(r,t) \tag{23}$$

where $p_l(t)$ is the pressure in the liquid phase (see Fig. 6). The value of $\chi(r,t)$ is given by:

$$\chi(r,t) = \gamma_{li}(t)\left(\frac{2}{R_{eq}(t)} - \frac{1}{r - \delta(t)}\right) \tag{24}$$

According to Eq. (23), the local pressure exerted by the ice crystal will be determined by the radius of the pore (from interface curvature effects). It should be emphasized that the value of $\chi(r,t)$ always remains positive whatever the conditions are. It should also be noted that, once equilibrium is reached, the pressure in the liquid is uniform all over the porous medium.

The ice formation process can induce local and transient differences in stress. For instance, at the vicinity of a free surface, the ice crystal is held at atmospheric pressure, and according to Eq. (23), the liquid water is depressed. In the inner part of the paste, ice formation and fluid transfer may generate hydraulic pressures and so, a transient state can appear where the liquid water (and eventually the solid phase) is under pressure. How-

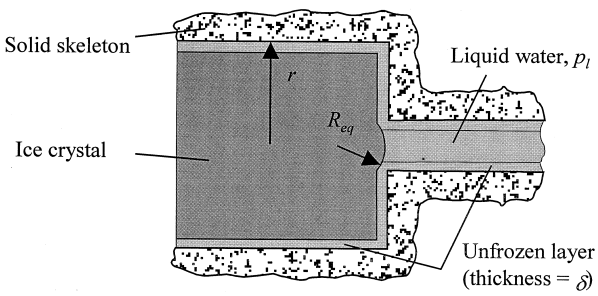

Fig. 6. Definition of the various variables appearing in Eq. (23).

ever, after a given period depending on the kinetics of the mass transfer, the pressure all over the ice crystal should be equal to the atmospheric pressure, and the liquid phase should be uniformly depressed by the value $\kappa(t)$ given by Eq. (21).

Depending on its size and on the current temperature, a pore is either filled with ice or saturated with liquid water. Let us call p^* the averaged pressure exerted by the ice crystals and the liquid phase on the pore walls [22,40–42]. According to this definition, p^* is equal to a weighted average over all possible radii r_k:

$$p^* = \sum_k p_k \frac{v_k}{V_p} \tag{25}$$

with

$$\frac{v_k}{V} = \frac{\mathrm{d}\varphi}{\mathrm{d}r}(r_k) \tag{26}$$

where v_k stands for the volume of pores of radius r_k. The total porosity (n) of the material is given by:

$$n = \frac{V_p}{V} = \lim_{r\to 0} \int_r^\infty \frac{\mathrm{d}\varphi}{\mathrm{d}r}\mathrm{d}r = \varphi(r_{\min}) \tag{27}$$

where $r_{\min}$ is the minimum pore radius of the solid (or the minimum pore radius that can be detected by a given technique).

In unfrozen pores, p_k is equal to p_l. In pores filled with ice, its value is equal to π_i. Therefore, by combining Eqs. (23), (25), (26) and (27), one can easily find that Eq. (28) holds true:

$$p^* = p_l + \frac{1}{n}\int_{R_{\mathrm{Peq}}(t)}^\infty \chi(r,t)\frac{\mathrm{d}\varphi}{\mathrm{d}r}\mathrm{d}r \tag{28}$$

If, in a first approximation, n is assumed to be constant during the freezing process (assumption which is not made when one writes Eq. (7)), one finds:

$$\dot{p}^* = \dot{p}_l + \frac{1}{n}\int_{R_{\mathrm{Peq}}(t)}^\infty \dot{\chi}(r,t)\frac{\mathrm{d}\varphi}{\mathrm{d}r}\mathrm{d}r \tag{29}$$

This last equation can be rewritten in a more general way as:

$$\dot{p}^*(t) = \dot{p}_l(t) + \dot{X}(t) \tag{30}$$

with $\dot{X}$ verifying Eq. (29), and thus Eq. (24).

3.3. Mechanical equilibrium of the porous medium

3.3.1. Mechanical description of the porous medium

Biot [43] has proposed an equation to describe the mechanical behavior of a porous material (partially) saturated with a liquid. This approach, based on the stress partition concept, rests on the assumption that the pore fluid and the solid skeleton both contribute to the stress state of the porous material. According to this approach, the relation between the effective elastic stress tensor: $\boldsymbol{\sigma}'$ and the total stress tensor $\boldsymbol{\sigma}$ (applied to the porous solid) is given by:

$$\boldsymbol{\sigma} = \boldsymbol{\sigma}' - bp^*\mathbb{I} \tag{31}$$

As previously defined (see Eq. (25)), p^* corresponds to the pore pressure.[2] $\mathbb{I}$ is the unit tensor. Similarly, the effective elastic stress tensor $\boldsymbol{\sigma}'$ corresponds to the fraction of the total stress carried by the porous solid. The parameter $\boldsymbol{b}$, called the Biot coefficient, is given by:

$$b = 1 - \frac{K}{K_s} \tag{32}$$

where K and K_s are the bulk modulus of the (drained) porous solid and that of the solid skeleton, respectively. According to this approach, the relation between the effective stress and the elastic strain is given by Eq. (33):

$$\boldsymbol{\sigma}' = \mathbb{C} : \boldsymbol{\epsilon}^e \tag{33}$$

where $\mathbb{C}$ is the elastic tensor of the (drained) porous material (that can be expressed as a function of the elastic modulus (E) and the Poisson coefficient (ν) of the porous solid).

The total strain tensor of the porous material, $\boldsymbol{\epsilon}$, is the sum of several contributions: the elastic strain tensor, $\boldsymbol{\epsilon}^e$, the thermal strain tensor $\boldsymbol{\epsilon}^{th}$, and, eventually, the irreversible strain tensor ($\boldsymbol{\epsilon}^{ir}$) [Eq. (34)]:

$$\boldsymbol{\epsilon} = \boldsymbol{\epsilon}^e + \boldsymbol{\epsilon}^{th}(+\boldsymbol{\epsilon}^{ir}) \tag{34}$$

For infinitesimal deformations, the following relation exists between the rate of volumetric strain, $\boldsymbol{\epsilon}$, and the velocity of the solid skeleton particles:

$$\mathrm{div}\boldsymbol{u} = \mathrm{tr}\left(\frac{\mathrm{d}\boldsymbol{\epsilon}}{\mathrm{d}t}\right) = \dot{\epsilon} \tag{35}$$

$\dot{\boldsymbol{\epsilon}}$ being the trace of the strain tensor $\boldsymbol{\epsilon}$.

3.3.2. Constitutive relations for the different phases

During the freezing process, the material is exposed to thermo-mechanical stresses. At the same time, the physical characteristics of the various phases present in the material evolve. Changes in density are then described by a constitutive relation, which links density to the thermal and mechanical variables that describe the problem.

The behavior of liquid water is described by two variables, its pressure and temperature [Eq. (36)]:

$$\delta\rho_l = \frac{\partial\rho_l}{\partial p_l}\delta p_l + \frac{\partial\rho_l}{\partial T}\delta T \tag{36}$$

The coefficient of isobaric volumetric thermal expansion of liquid water is defined as [Eq. (37)]:

$$\alpha_l = \frac{-1}{\rho_l}\left.\frac{\partial\rho_l}{\partial T}\right|_{p_l} \tag{37}$$

[2] According to our notation, a tensile stress is positive. A positive pressure corresponds to a compressive stress and is therefore negative.

The isothermal compressibility is also defined [Eq. (38)]:

$$K_l = \frac{+1}{\rho_l}\frac{\partial \rho_l}{\partial p_l}\bigg|_T \tag{38}$$

On the basis of these two definitions, one can write [Eq. (39)]:

$$\frac{1}{\rho_l}\frac{d\rho_l}{dt} = \frac{1}{K_l}\dot{p}_l - \alpha_l \dot{T} \tag{39}$$

Similarly, if ice is assumed to behave as a fluid (which, however, does not flow), one can write:

$$\frac{1}{\rho_i}\frac{d\rho_i}{dt} = \frac{1}{K_i}\dot{p}_i - \alpha_i \dot{T} \tag{40}$$

For the solid phase, constituting the solid skeleton, the density is a function of temperature and the applied stress. The total applied stress is a function of the effective stress and the pore pressure (as seen in Eq. (31)). Thus, the solid phase density depends on temperature, T, the effective stress, $\boldsymbol{\sigma}'$, and the pore pressure, $\boldsymbol{p}^*$.

Density is a volumetric variable. Therefore, the influence of the effective stress tensor, $\boldsymbol{\sigma}'$, is limited to the hydrostatic part of this tensor [Eq. (41)]:

$$\sigma'^{H} = \mathrm{tr}\boldsymbol{\sigma}'^{H} = \mathrm{tr}\left(\frac{\mathrm{tr}\boldsymbol{\sigma}'}{3}\mathbb{I}\right) = \mathrm{tr}\boldsymbol{\sigma}' \tag{41}$$

Since $\boldsymbol{\sigma}'$ is carried by the total volume of the porous material, its effect on the solid skeleton should be weighted by the inverse fraction of solid matrix ($(1)/(1-\boldsymbol{n})$) [29,44]. One can then find the constitutive relation for the solid phase [Eq. (42)]:

$$\frac{1}{\rho_s}\frac{d\rho_s}{dt} = \frac{1}{K_s}\dot{p}^* - \alpha_s \dot{T} - \frac{\mathrm{tr}\dot{\boldsymbol{\sigma}}'}{3(1-n)K_s} \tag{42}$$

The rate of volumetric strain of the porous material, $\dot{\boldsymbol{\epsilon}}$, is also a function of these three variables. Since we are concerned by the behavior of the complete porous skeleton, the effective strain effect is therefore linked to the drained characteristics of the porous material [Eq. (43)]:

$$\dot{\boldsymbol{\epsilon}} = \frac{1}{K_s}\dot{p}^* - \boldsymbol{\alpha}_s \dot{T} - \frac{\mathrm{tr}\dot{\boldsymbol{\sigma}}'}{3K} \tag{43}$$

Using these last two expressions with Eqs. (32) and (35), we find the relation:

$$\frac{1}{\boldsymbol{\rho}_s}\frac{d\boldsymbol{\rho}_s}{dt} = \left(\frac{b-n}{1-n}\right)\frac{\dot{p}^*}{K_s} - \left(\frac{b-n}{1-n}\right)\boldsymbol{\alpha}_s \dot{T} - \left(\frac{1-b}{1-n}\right)\mathrm{div}\boldsymbol{u} \tag{44}$$

4. Discussion

4.1. Final system of equations

By respectively substituting Eqs. (44) and (40) in Eqs. (7) and (8), which are then substituted in Eq. (6), and by using Eqs. (4), (19), (20) and (30), the resolution of Eq. (6) is equivalent to solving the following system of two equations [Eqs. (45) and (46)]:

$$\beta \dot{p}_l = \mathrm{div}\left(\frac{D}{\eta_l}\mathrm{grad}\, p_l\right) + S \tag{45}$$

and $\boldsymbol{u}$ solution of the mechanical equilibrium:

$$\mathrm{div}\boldsymbol{\sigma} = 0 \tag{46}$$

$\boldsymbol{\sigma}$ being the stress tensor defined in Section 3.3.1, with Eqs. (47)–(49) defining the following:

$$\beta = \frac{nS_l}{K_l} + \frac{nS_i}{K_i} + \frac{b-n}{K_s} \tag{47}$$

$$S = \left(1 - \frac{\rho_i}{\rho_l}\right)\Phi(t) + \overline{\alpha}\dot{T} - \frac{b-n}{K_s}\dot{X} - \frac{nS_i}{K_i}\dot{\kappa} - b\mathrm{div}\boldsymbol{u} + \frac{D}{\eta_l \rho_l}\mathrm{grad}\, p_l \mathrm{grad}\rho_l \tag{48}$$

$$\overline{\alpha} = nS_l\alpha_l + nS_i\alpha_i + (b-n)\alpha_s \tag{49}$$

$\Phi(t)$, $\kappa(t)$ and $X(t)$ being defined by Eqs. (18), (21) and (30), respectively.

As can be seen, the behavior of a saturated porous solid subjected to freezing temperatures can be described on the basis of a few, but relatively complex, equations. The intricate nature of this system of equations arises from the fact that the ice formation process is coupled to two other phenomena: transfer of liquid within the material pore structure and the mechanical response of the solid. A solution to this system of equations can be find numerically using the finite element method. The numerical resolution required for this system of non-linear equations will be discussed in another publication.

4.2. Determination of the input data

A reliable prediction of the behavior of a given porous material upon freezing is obviously linked to a good knowledge of a certain number of physical parameters. The input data required to run the model are listed in Table 1. The input parameters can be divided into three distinct categories:

1. the physical properties of the material;
2. the mechanical and thermal properties of ice; and
3. the physical properties of the interstitial liquid.

As can be seen in Table 1, most of the input parameters concern the physical properties of the porous solid. In order to run the model, one must first determine (or estimate) the mechanical properties of the porous solid. These properties include the elastic modulus (E) and the Poisson coefficient (ν) of the material. Both parameters can be determined experimentally. As indicated in the

Table 1
Input data of the modeling

Property	Symbol	Units	Value	References
Porous medium and solid skeleton				
• Elastic modulus of the porous body	E	[GPa]	≈ 20 for hardened cement paste	[63]
• Poisson's coefficient	ν	[−]	≈ 0.2	[63]
• Bulk modulus of the porous body	K	[GPa]	$K = E/(1-2\nu)$	[63]
• Total porosity	n	[m^3/m^3]	To be determined experimentally	
• Pore volume distribution	φ	[m^3/m^3]	To be determined experimentally	
• Initial permeability	D_0	[m^2]	To be determined experimentally	
• Bulk modulus of the solid skeleton	K_s	[GPa]	$K_s \approx (K/(1-n)^m)$, $m \approx 3$ for hardened cement paste	[3]
• Solid skeleton coefficient of volumetric thermal expansion	α_s	[$°C^{-1}$]	≈ 25	[46,47]
Liquid water and ice				
• Ice compressibility	K_i	[GPa]	≈ 8.34	[59]
• Water compressibility	K_l	[GPa]	≈ 2.18 for pure water	[58]
• Ice coefficient of volumetric thermal expansion	α_i	[$°C^{-1}$]	$\alpha_i(\theta) = 5.5(1+(\theta/200)) \times 10^{-5}$	[59]
• Liquid water coefficient of volumetric thermal expansion	α_l	[$°C^{-1}$]	$\alpha_l(\theta) = (-9.2+2.07\theta) \times 10^{-5}$	[59]
• Interstitial fluid dynamic viscosity	η_{ll}	[Pa s]	To be determined experimentally	[58]
• Ice/liquid water surface tension	γ_{li}	[N/m]	$\gamma_{li}(\theta) = (36+0.25\theta) \times 10^{-3}$	[32,58]

table, the bulk modulus (K) of the material (assumed to be isotropic) can be calculated using the following well-known relation [Eq. (50)]:

$$K = \frac{E}{3(1-2\nu)} \tag{50}$$

There exists in the literature very little information on the value of the bulk modulus of the solid skeleton (K_s) of hydrated cement systems. This value could eventually be deduced from the experimental data reported by Beaudoin [45] who measured the mechanical properties of hydrated cement compacts. According to Scherer [3], the value of (K_s) can also be estimated by the following relation [Eq. (51)]:

$$K_s = \frac{K}{(1-n)^m} \tag{51}$$

where m is roughly equal to 3 for hydrated cement pastes.

In the literature, a few authors have attempted to measure the coefficient of volumetric thermal expansion (α_s) of hydrated cement systems. The values reported are usually on the order of 25$(°C)^{-1}$ [46,47].

The use of the model also requires the determination of the initial permeability (D_0) of the material (i.e., the permeability of the unfrozen and undamaged solid). The permeability of porous cement systems (prepared at a water/cement ratio higher than 0.6) can be easily determined using simple experimental procedures. However, as emphasized by many authors [29,48–50], it is difficult to reliably measure the permeability of ordinary and high-performance cement systems. The use of two new promising techniques proposed by Scherer [51,52] to evaluate the value of D_0 will be briefly discussed in Part II. The discussion will also address the influence of ice formation on the permeability of hydrated cement systems.

The use of the model also requires the determination of the total porosity and the pore size distribution of the material. The total porosity can be easily measured experimentally. As previously mentioned, there is evidence that the pore size distribution of the material can be reasonably assessed by MIP measurements [32,38]. It should be noted that, in our case, the application of the technique does not suffer from the many disadvantages usually discussed in the literature [53–55]. In fact, the technique is particularly well adapted since it provides information on the distribution of the pore entry radii.

However, special care should be taken to minimize the damage induced to the material microstructure by the required predrying treatment. The hydrated cement paste is a moisture-sensitive body and numerous publications have clearly emphasized that even mild drying treatments can significantly modify the material pore structure, and, therefore, the ice formation process [19,33,56,57]. Various techniques to reduce the detrimental influence of drying are discussed in Ref. [55].

As indicated in Table 1, in order to run the model, one also has to input values for various properties of the interstitial fluid. Textbook values for the compressibility of liquid water are usually on the order of 2.18 GPa [58]. Information on the values of temperature-dependent properties, such as the volumetric thermal expansion of water and the ice/liquid water surface tension, can also be found in the literature [32,58,59]. The following empirical relation is proposed in the literature to estimate the variation

of the dynamic viscosity of the fluid between 20°C and −20°C [58]:

$$\eta_l = \log_{10}(10^3\eta_l(\theta)) = \frac{1301}{998.333 + 8.1855(\theta - 20) + 0.00585(\theta - 20)^2} - 1.30233 \quad (52)$$

In this equation [Eq. (52)], θ stands for the temperature of the liquid water.

Similarly, one also needs to input the physical properties of ice. It has been reported that, upon normal freezing conditions, pore water in cement systems transforms mainly to hexagonal ice (type Ih) [60,61]. The thermal and mechanical properties of this type of ice can be found in many textbooks [58,59].

In a first approximation, the difference between the density of liquid water and that of ice may be kept constant and equal to a 9% volume expansion when solidification occurs. The term linked to ice formation into Eq. (18) can be evaluated to [Eq. (53)]

$$\left(1 - \frac{\rho_i}{\rho_l}\right)\Phi(t) = \left(1 - \frac{1}{1.09}\right)\Phi(t) = 0.0826\Phi(t) \quad (53)$$

This value of 0.0826 was the one used, for instance, in Ref. [62].

4.3. Basic assumptions

As in many other similar cases, this model was developed from a certain number of basic assumptions. These assumptions can be divided into three categories:

1. assumptions related to the thermal regime of the system;
2. an assumption related to the pore shape; and
3. an assumption related to the estimation of the mean pore pressure.

The first category includes three different assumptions. The first one concerns the temperature distribution within the material. The model rests on the assumption that the entire system is kept under isothermal conditions (i.e., that no thermal gradients are developed within the material upon freezing). Obviously, this assumption limits the size of the samples that can be considered to a few cubic centimeters. However, our mesoscopic model is sufficient to study the influence of various material parameters (such as air entrainment, water/cement ratio, ...) on the frost resistance of the solid.

In this approach, any temperature change resulting from the exothermal ice formation process is also neglected. This effect should be minimal if the characteristic volume of the sample is limited to a few cubic centimeters. In these conditions, the heat generated by the ice formation should dissipate very quickly.

The third assumption related to the thermal regime that has been previously discussed in Section 3.2. It concerns the fact that the rate of freezing is assumed to be relatively low (i.e., no more than 5°C per hour). Under these conditions, the rate of ice formation is directly controlled by the rate of freezing. As previously emphasized, this assumption is usually verified for most concrete structures exposed to natural conditions. Furthermore, the freezing rates specified for most standardized laboratory procedures (such as ASTM C671) rarely exceed this limit.

The second category of assumptions concerns the shape of the pores found in the material. Such a hypothesis is only made in the calculation of the volume of unfrozen water (see Eqs. (15) and (16)) where the pores were assumed to be cylindrical in shape). However, as previously emphasized, the pore shape has only a secondary influence on the numerical results. It should also be noted that Eqs. (9) and (12), which allow the calculation of $R_{p_{eq}}$, were developed by assuming the propagation of a spherical interface through the material pore structure. However, as discussed by some authors [32,39], this assumption is valid for any shape of pore.

The last assumption concerns the determination of p^* (see Eq. (25)). The calculation is made by averaging the contribution of each class of pores found in the solid. This assumption is based first on the fact that, due to the importance of the surface of contact, the liquid and the solid phases are in thermodynamic equilibrium [26,28,30]. Furthermore, from a micromechanical consideration, each pore can be considered to act as an independent inclusion [22,40–42].

It should also be noted that the model was developed assuming that the porous solid was initially saturated. The approach could, however, be modified to account for the presence of a vapor phase. The treatment of partially saturated porous solids by a poro-elastic approach has been recently discussed by many authors [26–28,30,31].

It should finally be emphasized that this model does not account for the influence of the progressive degradation of the material. This effect could eventually be treated without any significant modification of the actual structure of the model. However, this would require developing phenomenological relations to account for the evolution of damage upon freezing.

5. Conclusions

A model to predict the behavior of hydrated cement systems subjected to freezing temperatures was developed. The model was derived from thermodynamic and kinetic considerations. All equations were written at the microscopic scale and then averaged over an elementary representative volume of the material (mesoscopic scale).

The system of equations was built in such a way as to predict temperature-induced phase transitions and the resulting transfers of mass within the material pore structure. The model also yields the local pressures generated in the liquid and solid phases by mass transfer and crystal growth. The system of non-linear equations is solved numerically.

Acknowledgments

The authors are grateful to the Natural Sciences and Engineering Research Council of Canada (NSERC) and Ecole normale Supérieure de Cachan for their financial support for this project. The authors would also like to thank Dr. J.J. Beaudoin, Dr. E.J. Garboczi, Mr. K.A. Snyder, Prof. G. Pijaudier-Cabot, Prof. F. Hild and Prof. G. Scherer for several useful discussions during the course of this research.

References

[1] J. Marchand, R. Pleau, R. Gagné, Deterioration of concrete due to freezing and thawing, in: S. Mindess, J. Skalny (Eds.), Material Science of Concrete, Vol. 4, Am Ceram Soc, Westerville, OH, USA, 1995, pp. 283–354.
[2] G.G. Litvan, Phase transitions of adorbates: Part VI. Effect of deicing agents on the freezing of cement paste, J Am Ceram Soc 58 (1–2) (1975) 26–30.
[3] G.W. Scherer, Proposed mechanism for salt scaling, Cem Concr Res, 2000 (to be submitted for publication; 32 pp.).
[4] G.W. Scherer, Crystallization in pores, Cem Concr Res 29 (8) (1999) 1347–1358.
[5] G.W. Scherer, Freezing gels, J Non-Cryst Solids 155 (1993) 1–25.
[6] T.C. Powers, The air requirement of frost-resistant concrete, in: Proceedings of the Highway Research Board, PCA Bulletin 33, Portland Cement Association, Skokie, Il, Vol. 29, 1949, pp. 184–211.
[7] T.C Powers, R.A. Helmuth, Theory of volume changes in hardened Portland cement paste, in: Proceedings of the Highway Research Board, PCA Bulletin 46, Portland Cement Association, Skokie, Il, Vol. 32, 1953, pp. 285–297.
[8] R.F. Feldman, Length change–adsorption relations for the water-porous glass system to −40°C, Can J Chem 42 (2) (1970) 287–297.
[9] G.G. Litvan, Phase transitions of adsorbates: Part IV. Mechanism of frost action in hardened cement paste, J Am Ceram Soc 55 (1) (1972) 38–42.
[10] J.-M. Konrad, C. Duquennoi, A model for water transport and ice lensing in freezing soils, Water Resour Res 29 (9) (1993) 3109–3124.
[11] R.R. Gilpin, A model for the prediction of ice lensing and frost heave in soils, Water Resour Res 16 (5) (1980) 918–930.
[12] S. Jacobsen, Scaling and cracking in unsealed freeze/thaw testing of Portland cement and silica fume concretes, PhD thesis, Department of Civil Engineering, University of Trondheim, Norway, 1995, 286 pp.
[13] J. Marchand, E.J. Sellevold, M. Pigeon, The deicer salt scaling deterioration of concrete — an overview, ACI SP-145 (1994) 1–46.
[14] M.C. Laroche, J. Marchand, M. Pigeon, Reliability of the ASTM C 672 test procedure, in: J. Marchand, M. Pigeon, M.J. Setzer (Eds.), Freeze–thaw Durability of Concrete, E&FN Spon, London, UK, 1996, pp. 199–210.
[15] T. Sedran, M. Pigeon, K. Hazrati, The influence of penetrating sealers on the deicer salt scaling resistance of concrete, in: S. Nagataki, T. Nireki, F. Tomosawa (Eds.), Proceedings of the 6th International Conference on Durability of Building Materials and Components, Omiya, Japan, London, UK, 1993, pp. 487–496.
[16] M. Pigeon, J. Marchand, The frost durability of roller-compacted concrete, Concr Int 18 (7) (1996) 22–27.
[17] J. Marchand, R. Gagné, S. Jacobsen, M. Pigeon, E.J. Sellevold, The frost durability of high-performance concrete, Can J Civ Eng 23 (1996) 1070–1080 (in French).
[18] G. Fagerlund, Frost resistance of high performance concrete — some theoretical considerations, Report TVBM-3056, Division of Building Materials, Lund Institute of Technology, 1993, p. 38.
[19] B. Zuber, J. Marchand, A. Delagrave, J.-P. Bournazel, Ice formation mechanisms in normal and high-performance concrete mixture, ASCE J Mater Civ Eng 12 (1) (2000) 16–23.
[20] J. Marchand, L. Boisvert, S. Tremblay, J. Maltais, M. Pigeon, Air entrainment in dry concrete mixtures, Concr Int 20 (4) (1998) 38–44.
[21] Z.P. Bažant, J.C. Chern, A.M. Rosenberg, J.M. Gaidis, Mathematical model for freeze–thaw durability of concrete, J Am Ceram Soc 71 (9) (1988) 776–783.
[22] B. Zuber, Modeling the mechanisms of frost degradation of hydrated cement systems, PhD thesis, Department of Civil Engineering, Université Laval/Ecole Normale Supérieure de Cachan, 2000 (in preparation; in French).
[23] M. Hassanizadeh, W.G. Gray, General consideration equations for multiphase system: Part 1. Averaging technique, Adv Water Resour 2 (1979) 131–144.
[24] M. Hassanizadeh, W.G. Gray, General consideration equations for multiphase system: Part 2. Mass, momenta, energy and entropy equations, Adv Water Resour 2 (1979) 191–201.
[25] M. Hassanizadeh, W.G. Gray, General consideration equations for multiphase system: Part 3. Constitutive theory for porous media flow, Adv Water Resour 3 (1980) 25–40.
[26] W.G. Gray, M. Hassanizadeh, Unsaturated flow theory including interfacial phenomena, Water Resour Res 27 (1991) 1855–1863.
[27] D. Gawin, P. Baggio, B.A. Schrefler, Coupled heat, water and gas flow in deformable porous media, Int J Numer Methods Fluids 20 (1995) 969–987.
[28] O. Coussy, Mechanics of Porous Continua, Wiley, 1995, Chichester, UK, p. 455.
[29] B. Bary, Study of hydro-mechanical couplings in damaged concrete, PhD thesis, Lab de Mécanique et Technologie, Ecole normale supérieure de Cachan, 1996, p. 156 (in French).
[30] Z.P. Bažant, Analysis of pore pressure, thermal stress and fracture in rapidly heated concrete, in: G. Fronsdhorff, N. Carino, E.J. Garboczi, (Eds.), Proceedings of the International Workshop on Fire Performance of High-Strength Concrete, Papers B. 10, NIST Gaithersburgh, MD, USA, 1997, pp. 155–164.
[31] B.A. Schrefler, L. Sanavia, C.E. Majorana, A multiphase medium model for localisation and postlocalisation simulation in geomaterials, Mech Cohesive-Frict Mater 1 (1996) 95–114.
[32] S. Matala, Effects of carbonation on the pore structure of granulated blast furnace slag concrete, PhD thesis, Rep. 6, Helsinki University of Technology, Faculty of the Civil Engineering and Surveying Concrete Technology, Espoo, Finland, 1995, p. 161.
[33] E.J. Sellevold, D.H. Bager, Some implications of calorimetric ice formation results for frost resistance testing of cement products, Tech. Rep. 86/80, The Technical University of Denmark, 1980, p. 28.
[34] G. Fagerlund, Determination of pore-size distribution from freezing-point depression, Mater Struct 6 (33) (1973) 215–225.
[35] D.H. Bager, E.J. Sellevold, Ice formation in hardened cement paste: Part I. Room temperature cured paste with variable moisture contents, Cem Concr Res 16 (5) (1986) 709–720.
[36] F. Radjy, Thermodynamic parameters for sorption of water by hardened cement, Paper No. 6 presented at the 77th Annual Meeting of the American Ceramic Society, Cements Division, Washington, DC, USA, 1975, p. 10.
[37] E.J. Garboczi, D.P. Bentz, Digitized simulation of mercury intrusion

porosimetry, in: S. Mindess (Ed.), Advances in Cementitious Materials, Ceram Trans, Vol. 16, Am Ceram Soc, Westerville, OH, USA, 1990, pp. 365–379.
[38] J. Villadsen, The influence of curing temperature on pore structure of hardened cement paste, Lab for Bygn Mat, Danmarks Tekn. Hjskole, Techn. Rep. 218/90, 1989.
[39] M. Brun, A. Lallemand, J.-F. Quinson, C. Eyraud, A new method for the simultaneous determination of the size and shape of pores: The thermoporometry, Thermochim Acta 21 (1977) 59–88.
[40] F. Hild, Damage, fracture and scale change in heterogeneous materials, Thesis, Université Pierre et Marie Curie, Paris 6, Lab de Mécanique et Technologie, Ecole normale supérieure de Cachan, France, 1998, p. 324 (in French).
[41] T. Mura, Micromechanics of Defects in Solids, Martinus Nijhoff Publishers, 1982, p. 494.
[42] S. Nemat-Nasser, M. Hori, Micromechanics: Overall properties of heterogeneous materials, in: J.D. Achenbach, B. Budianski, H.A. Lauwerier, P.G. Saffman, L. Van Wijngaarden, J.R. Willis (Eds.), North-Holland Series in Applied Mathematics and Mechanics, Elsevier, Amsterdam, 1993, p. 687.
[43] M.A. Biot, General theory of three-dimensional consolidation, J Appl Phys 12 (1941) 55–164.
[44] L. Xikui, Finite-element analysis for immiscible two-phase fluid flow in deforming porous media and an unconditionally stable staggered solution, Comm Appl Numer Methods 6 (2) (1990) 125–135.
[45] J.J. Beaudoin, Comparison of mechanical properties of compacted calcium hydroxide and portland cement paste systems, Cem Concr Res 22 (1983) 707–718.
[46] R.A. Helmuth, Capillary size restrictions on ice formation in hardened cement paste, in: Proceedings of the 4th International Congress on the Chemistry of Cements, Washington, DC, USA, Portland Cement Association, Skokie, Il, 1960, Vol. 2, pp. 855–869 (Monograph 43, Session VI, Paper VI-S2).
[47] V.E. Penttala, Freezing-induced strains and pressures in wet porous materials and especially in concrete mortars, Adv Cem Based Mater 7 (1998) 8–19.
[48] A.S. El-Dieb, R.D. Hooton, Water permeability measurements of high-performance concrete using a high-pressure triaxial cell, Cem Concr Res 25 (1995) 1199–1208.
[49] E.J. Garboczi, Permeability, diffusivity and microstructural parameters: A critical review, Cem Concr Res 20 (1990) 503–514.
[50] J. Marchand, B. Gérard, Microstructure-based models for predicting transport properties, in: K. Scrivener, J.F. Young (Eds.), Penetration and Permeability of Concrete, E&FN Spon, London, UK, 1997, pp. 41–81.
[51] G. Scherer, Thermal expansion kinetics: Method to measure the permeability of cementitious material: Part 1. Theory, J Am Ceram Soc (in press).
[52] G. Scherer, Measuring the permeability of rigids materials by a beam-bending method: Part 1. Theory, J Am Ceram Soc 83 (9) (2000) 2231–2239.
[53] S. Diamond, Methodologies of pore size distribution measurements in hydrated cement pastes: Postulates, pecularities, and problems, Mater Res Soc Proc 137 1989, pp. 83–89.
[54] S. Diamond, M.E. Leeman, Pore size distributions in hardened cement paste by SEM image analysis, Mater Res Soc Proc 376 (1995) 217–226.
[55] J.J. Beaudoin, J. Marchand, Pore structure, in: V.S. Ramachandran, J.J. Beaudoin (Eds.), Handbook of Analytical Techniques in Concrete Science and Technology, Noyes Publishing, New York, NY, USA, 2000 (in press).
[56] D.H. Bager, E.J. Sellevold, Ice formation in hardened cement paste: Part II. Drying and resaturation of room temperature cured paste, Cem Concr Res 16 (1986) 835–844.
[57] J.J. Beaudoin, P. Gu, P.J. Tumidajski, S. Perron, Microstructural changes on drying and rewetting of hydrated cement paste — an A.C. impedance spectroscopy study, in: J.P. Bournazel, Y. Malier (Eds.), Concrete: From Material to Structure, RILEM, London, UK, 1998, pp. 207–238.
[58] R.C. Weast, M.J. Astle, W.H. Beyer (Eds.), CRC Handbook of Chemistry and Physics, 66th edn., CRC Press, Boca Raton, FL, USA, 1986.
[59] P.V. Hobbs, Ice Physics, Clarendon Press, Oxford, UK, 1974, p. 837.
[60] M.J. Setzer, Interaction of water with hardened cement paste, in: S. Mindess (Ed.), Advances in Cementitious Materials, Am Ceram Soc Trans, Vol. 16, American Ceramic Society, Westerville, OH, USA, 1990, pp. 415–439.
[61] E.M. Schulson, I.P. Swainson, T.M. Holden, C.J. Korhonen, Ice Ih in hardened cement, Cem Concr Res 30 (2) (2000) 191–196.
[62] O. Katsura, E. Kamada, A mechanism of frost damage of concrete under supercooling, in: M.J. Stezer, R. Auberg (Eds.), Frost Resistance of Concrete, E&FN Spon, London, 1997, pp. 202–211.
[63] J. Lemaître, J.-L. Chaboche, Mécanique des Matériaux Solides, 2nd edn., Dunod, Paris, France, 1988 (544 pp.; in French).